J. Fluid Mech. (2005), *vol.* 528, *pp.* 43–52.
doi:10.1017/S0022112005003307 Printed in the United Kingdom

Transient growth in two-phase mixing layers

By P. YECKO[1,2] AND S. ZALESKI[3]

[1]Department of Astronomy, Columbia University, 550 West 120th Street, New York, NY 10027, USA

[2]Department of Mathematics, Massachusetts Institute of Technology, Cambridge, MA 02139, USA

[3]Laboratoire de Modelisation en Mécanique, Université Pierre et Marie Curie (Paris VI), 4 Place Jussieu, 75252 Paris, France

(Received 23 October 2004 and in revised form 15 December 2004)

Transient growth properties are computed for a two-phase temporal mixing layer of immiscible fluids with interfacial tension. Large transient growth factors are found to occur at short times in parameter regimes characteristic of the primary breakup of a liquid. Optimal growth factors scale with the square of the Reynolds number, as for single-phase flow. The flow fields of optimal disturbances show liquid upflows and high-speed streamwise gas jets occurring together near the interface, suggesting transient growth as a possible mechanism for the formation of interfacial patterns. Optimal growth occurs for streamwise uniform disturbances with a spanwise wavelength proportional to the thickness of the gas boundary layer. For a coaxial jet, the predicted number of ligaments would be inversely proportional to the gas boundary layer thickness.

1. Introduction

The deformation and disintegration of a liquid by a fast flowing gas is a phenomenon of fundamental importance in both nature and industry. Noteworthy examples include the wind-driven formation of sea spray, an important component of sea surface material and heat fluxes, and the atomization of liquids, such as fuels in combustion applications (Lefebvre 1989; Bayvel & Orzechowski 1994). Experiments in which high-speed co-flowing gas drives the breakup of liquid jets (Mayer 1994; Lasheras & Hopfinger 2000; Marmottant & Villermaux 2004, referred to herein as MV), liquid sheets (Mansour & Chigier 1990; Stapper, Sowa & Samuelson 1992; Lozano *et al.* 2001) and liquid layers (Raynal 1997) have revealed two co-existing patterns on the interface at early times: (i) a growing spanwise vortical wave, apparently generated by the shear at the interface; and (ii) a streamwise vortical pattern that can lead to protruding streamwise oriented ligaments (SOL), as sketched in figure 1(*a*). These ligaments are precursors of drop formation and their three-dimensional nature precludes an explanation via two-dimensional stability analysis. Stapper *et al.* (1992) also found that streamwise vorticity is associated with the streamwise ligamentary pattern.

Liquid injected at high speed into quiescent gas also exhibits SOL, a configuration studied extensively by Faeth and co-workers in both cylindrical and planar jet geometries (see also Hoyt & Taylor 1977 and Sarpkaya & Merrill 2001) and for which a turbulent primary breakup theory has been developed (Wu, Miranda & Faeth 1995) that successfully correlates ligament properties with the scales of developed

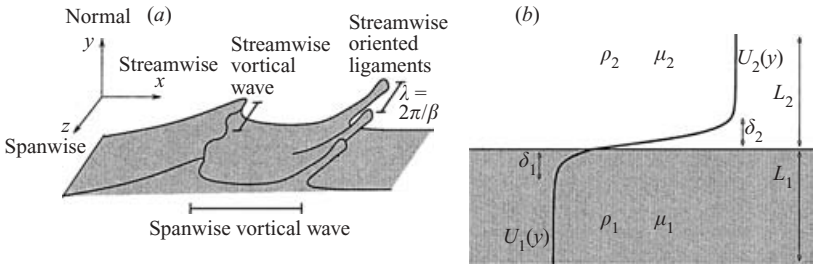

FIGURE 1. Sketches showing: (*a*) streamwise and spanwise patterns; and (*b*) the base flow.

turbulence in the liquid. This theory cannot, however, address the essentially laminar flow experiments, like those of MV, nor is it strictly applicable when turbulence is not fully developed, as in many applications of interest (e.g. diesel fuel injectors).

Streamwise vorticity in single-phase shear flows has been intensely examined for its role in the transition to turbulence. It is now clear, for example, that streamwise vortices in boundary layers are responsible for the high- and low-speed streamwise streaks seen at moderate Reynolds numbers (a high-speed streak is formed as a streamwise vortex pushes fast fluid from the free stream down into the boundary layer). Streamwise vortices are not a consequence of modal instability, rather they result from the transient growth of optimal disturbances – special initial conditions which experience large transient amplification. There is not space here to review this active topic; the interested reader can find a comprehensive review and bibliography in Schmid & Henningson (2000). Transient growth theory has been more successful than eigenvalue analysis in describing aspects of transition in pipe flow, channel flow and some types of boundary layers.

To date, stability analyses of co-flowing liquid and gas – whether jets, sheets or layers – have been almost entirely restricted to eigenvalue studies. On the one hand, this is justified by the fact that a Kelvin–Helmholtz-type instability (the spanwise vortical/interfacial mode) is found and its predicted characteristics show reasonably good agreement with observations. On the other hand, eigenvalues describe the asymptotic stability of a flow whereas the breakup of liquids is a rapid process, for which transient instability may be equally pertinent. A few investigations of transient growth in a two-fluid shear flow have been performed: three-dimensional computations were made by Olsson & Henningson (1995) for watertable flow, neglecting the less dense layer; and de Luca, Costa & Caramiello (2002) examined a liquid sheet falling through a still, inviscid gas. Two-dimensional studies have also been made: South & Hooper (1999) focus on the case of uniform density and neglect surface tension while Noorden *et al.* (1998) account for both non-uniform density and surface tension.

The primary purpose of this work is to present, for the first time, characteristics of three-dimensional transient growth in a two-phase shear flow in which capillary forces act on the interface. We have chosen an unbounded temporal mixing layer configuration which admits a straightforward computation of transient growth properties and which is relevant to a number of atomization problems for which the characteristic length scales are much smaller than the flow geometry. Densities and viscosities are chosen to correspond to a wide range of gas–liquid combinations, including the air–water case; density-matched flow is not considered here. This work has been partly motivated by the need to understand streamwise oriented ligament formation in liquid breakup, and guided by the tendency of transient growth to generate streamwise patterns.

Recently, Marmottant & Villermaux (2004, henceforth referred to as MV), have performed experiments on co-axial jets using a range of liquids and carefully prepared exit profiles (see also the earlier studies of Lasheras, Villermaux & Hopfinger 1998). MV analysed the resulting spanwise wave and streamwise ligament formation and presented a theory which agrees with a number of observed trends. In this work, we arrive at an alternative model that provides spanwise periodic structure consistent with the properties of SOL as a result of the transient growth of optimal disturbances.

2. Base flow

The base flow consists of two immiscible fluids flowing in parallel and separated by a flat interface; the domain extends to $\pm\infty$ in our theoretical treatment, but is truncated for computational purposes at large finite values $-L_1$ and L_2 (see figure 1*b*). The fluids are incompressible, Newtonian and satisfy the Navier–Stokes equations; they have different viscosities μ_j and densities ρ_j (where $j=1,2$ and $\nu_j=\mu_j/\rho_j$) and a surface tension σ acts on the interface. Gravity is neglected. The base velocity profile $\bar{\boldsymbol{u}}=(U_j,0,0)$ is the solution of the First Stokes Problem, here in the form $U_j(y)=U_j^*\mathrm{erf}(y/\delta_j)$, such that the interface is located at $y=0$ and has zero velocity; base pressure is constant: $\bar{p}=p^*$. The First Stokes solution is time-dependent, its boundary layer thickness given by $\delta_j=3.6\sqrt{\nu_j t}=(\delta_{99})_j$ (Schlichting & Gersten 2000). We nevertheless perform an analysis of this profile at a particular snapshot in time, with the caveat that any growth, to be considered relevant, must occur more quickly than the boundary layers develop.

Continuity of tangential stress on the interface can be expressed as $U_2^*\mu_2/\delta_2=U_1^*\mu_1/\delta_1$, implying that the base velocity gradient (equivalently, vorticity) is discontinuous, unless the fluid viscosities are equal. The base flow is subject to both inviscid (i.e. Kelvin–Helmholtz type) and viscous instabilities, as previously studied in Yecko, Zaleski & Fullana (2002) and Boeck & Zaleski (2004). This temporal mixing layer is Galilean invariant and, in principle, may be applied to a wide range of liquid–gas flow configurations, including atomization of liquid by high-speed co-flowing gas and atomization of high-speed liquid injected into initially still gas.

Assuming that the boundary layers develop from the same initial time (SIT), their thicknesses always have a fixed ratio. We define $n:=\delta_2/\delta_1$ and then have $n=(\nu_2/\nu_1)^{1/2}$. The SIT assumption is discarded in § 5.3, where we compare our results to experiments.

Non-dimensionalization may be performed with respect to either liquid or gas quantities; here, we use the free-stream liquid velocity U_1^*, liquid boundary layer thicknesses δ_1 and pressure $\rho_1(U_1^*)^2$. The resulting (liquid) Reynolds number is based on the boundary layer thickness and is given as $Re_1=\rho_1U_1^*\delta_1/\mu_1$ while the Weber number is $We_1=\rho_1(U_1^*)^2\delta_1/\sigma$. We introduce the density ratio $r=\rho_2/\rho_1$ and viscosity ratio $m=\mu_2/\mu_1$, from which expressions for the (gas) values $Re_2=(rn^2/m^2)Re_1$ and $We_2=(rn^3/m^2)We_2$ can be easily derived. Since $n=(m/r)^{1/2}$ is fixed, four dimensionless parameters are therefore needed; we take Re_1, We_1, r, and m.

3. Governing equations

The base state is perturbed by adding an infinitesimal disturbance of the form

$$(\boldsymbol{u}_j,\,p_j)=(\hat{\boldsymbol{u}}_j(y,t),\,\hat{p}_j(y,t))\mathrm{e}^{\mathrm{i}(\alpha x+\beta z)}. \tag{3.1}$$

The linear equations that govern the behaviour of these perturbations can be written in terms of the normal velocity $\hat{v}_j$ and normal vorticity $\hat{\eta}_j=\mathrm{i}\beta\,\hat{u}_j-\mathrm{i}\alpha\,\hat{w}_j$:

$$\frac{\partial}{\partial t}(\mathrm{D}^2-k^2)\hat{v}_j+\mathrm{i}\alpha U_j(\mathrm{D}^2-k^2)\hat{v}_j-\mathrm{i}\alpha\mathrm{D}^2U_j\hat{v}_j-\frac{1}{Re_j}(\mathrm{D}^2-k^2)^2\hat{v}_j=0, \tag{3.2}$$

$$\frac{\partial}{\partial t}\hat{\eta}_j + \mathrm{i}\alpha U_j \hat{\eta}_j + \mathrm{i}\beta \mathrm{D}U_j \hat{v}_j - \frac{1}{Re_j}(\mathrm{D}^2 - k^2)\hat{\eta}_j = 0 \tag{3.3}$$

where $k^2 = \alpha^2 + \beta^2$, $\mathrm{D} = \mathrm{d}/\mathrm{d}y$, and boundary conditions: $\hat{v}_j = \mathrm{D}\hat{v}_j = \hat{\eta}_j = 0$ hold far from the interface ($y \to \infty$). Re_j are fixed here; only the perturbations are time-dependent. The interface displacement f can be introduced by means of the kinematic condition

$$\frac{\mathrm{d}f}{\mathrm{d}t} = (\partial_t + \mathrm{i}\alpha U_j) f = \hat{v}_j(y = 0). \tag{3.4}$$

We introduce $\boldsymbol{q} = \tilde{\boldsymbol{q}}\mathrm{e}^{-\mathrm{i}\omega t}$, where $\tilde{\boldsymbol{q}} = (v_2(y), \eta_2(y), f, v_1(y), \eta_1(y))^T$, to have a more compact notation. An eigenvalue problem can then be written: $\mathrm{i}\omega \boldsymbol{M}\tilde{\boldsymbol{q}} = \boldsymbol{L}\tilde{\boldsymbol{q}}$, where

$$\boldsymbol{M} = \begin{pmatrix} \mathrm{D}^2 - k^2 & 0 & 0 & 0 & 0 \\ 0 & 1 & 0 & 0 & 0 \\ 0 & 0 & 1 & 0 & 0 \\ 0 & 0 & 0 & \mathrm{D}^2 - k^2 & 0 \\ 0 & 0 & 0 & 0 & 1 \end{pmatrix}, \quad \boldsymbol{L} = \begin{pmatrix} \mathscr{O}_2 & 0 & 0 & 0 & 0 \\ \mathscr{R}_2 & \mathscr{S}_2 & 0 & 0 & 0 \\ 0 & 0 & \mathrm{i}\alpha U_j & -1 & 0 \\ 0 & 0 & 0 & \mathscr{O}_1 & 0 \\ 0 & 0 & 0 & \mathscr{R}_1 & \mathscr{S}_1 \end{pmatrix}, \tag{3.5}$$

and the matrix elements are:

$$\mathscr{O}_j = \mathrm{i}\alpha U_j(\mathrm{D}^2 - k^2) - \mathrm{i}\alpha \mathrm{D}^2 U_j - \frac{1}{Re_j}(\mathrm{D}^2 - k^2)^2, \tag{3.6}$$

$$\mathscr{S}_j = \mathrm{i}\alpha U_j - \frac{1}{Re_j}(\mathrm{D}^2 - k^2), \qquad \mathscr{R}_j = \mathrm{i}\beta \mathrm{D}U_j\ . \tag{3.7}$$

Using the above, we can define the matrix operator $\mathscr{L}$ as $\boldsymbol{M}^{-1}\boldsymbol{L}\tilde{\boldsymbol{q}}_j = \mathscr{L}\tilde{\boldsymbol{q}}_j$.

On the interface, six matching conditions apply, corresponding to continuity of the three components each of velocity and stress. At $y = 0$ the normal velocity v_j, the streamwise velocity $u_j = \mathrm{i}k^{-2}(\alpha \mathrm{D}v_j - \beta\eta_j)$, and the spanwise velocity $w_j = \mathrm{i}k^{-2}(\beta \mathrm{D}v_j + \alpha\eta_j)$ must satisfy, respectively, the following:

$$v_2 = v_1, \tag{3.8}$$

$$(\omega - \alpha U)[\alpha(\mathrm{D}v_1 - \mathrm{D}v_2) - \beta(\eta_1 - \eta_2)] = k^2(\mathrm{D}U_2 v_2 - \mathrm{D}U_1 v_1), \tag{3.9}$$

$$\beta(\mathrm{D}v_1 - \mathrm{D}v_2) = \alpha(\eta_2 - \eta_1)\ . \tag{3.10}$$

At $y = 0$ the tangential stress components τ_{xy} and τ_{yz} must satisfy

$$m(\alpha(\mathrm{D}^2 + k^2)v_2 - \beta \mathrm{D}\eta_2 - \mathrm{i}k^2 \mathrm{D}^2 U_2 f) = \alpha(\mathrm{D}^2 + k^2)v_1 - \beta \mathrm{D}\eta_1 - \mathrm{i}k^2 \mathrm{D}^2 U_1 f, \tag{3.11}$$

$$m(\beta(\mathrm{D}^2 + k^2)v_2 + \alpha \mathrm{D}\eta_2) = \beta(\mathrm{D}^2 + k^2)v_L + \alpha \mathrm{D}\eta_1, \tag{3.12}$$

while the normal stress τ_{yy} condition is

$$r(\omega \mathrm{D}v_2 + \alpha \mathrm{D}U_2 v_2) - (\omega \mathrm{D}v_1 + \alpha \mathrm{D}U_1 v_1) + \frac{m(\mathrm{D}^3 v_2 - 3k^2 \mathrm{D}v_2)}{\mathrm{i}Re_1} - \frac{(\mathrm{D}^3 v_1 - 3k^2 \mathrm{D}v_1)}{\mathrm{i}Re_1} = -\frac{k^4}{\mathrm{i}We_1} f. \tag{3.13}$$

This disturbance problem is used below to calculate the complete spectrum of eigenfunctions and disturbances built from the eigenfunctions which experience the greatest transient amplification.

4. Computing transient growth

A Chebyshev collocation code developed in previous work (Yecko *et al.* 2002) was used to evaluate the eigenvalue stability problem defined above. Solutions for the spectrum are obtained in order to perform the transient amplification calculations, implementing the method given in Reddy & Henningson (1993). The linear problem is mapped to the Chebyshev interval $[-1, 1]$ and the eigenfunctions can then be written as an expansion in a finite number N of Chebyshev terms $T_n(y)$ with unknown expansion coefficients, where N is typically 150 or less. The eigenvalue problem is transformed into a corresponding $(4N+1)\times(4N+1)$ matrix problem for the expansion coefficients including the boundary and matching conditions. Because of the infinite domain a continuous spectrum is present in addition to the finite discrete spectrum. In the calculations performed here, each semi-infinite domain was approximated with a finite domain by choosing large values of L_1 and L_2, these values determined by finding insensitivity of computed results to increases in L_1 or L_2; the continuum is thus replaced by a discrete approximation.

Following the formulation of transient growth used in Schmid & Henningson (2000), let $G(t)$ represent the maximum possible energy amplification at time t, where G is optimized over all possible initial conditions for each instant in time. To measure the energy we require an appropriate norm; in this problem we use

$$||q||_E = \frac{1}{2k^2}\left[\int_{-L_1}^{0}(|\mathrm{D}v_1|^2 + k^2|v_1|^2 + |\eta_1|^2)\,\mathrm{d}y + r\int_{0}^{L_2}(|\mathrm{D}v_2|^2 + k^2|v_2|^2 + |\eta_2|^2)\,\mathrm{d}y + S\right] \quad (4.1)$$

where $S = k^4|f|^2/We_1$ is the interfacial energy, proportional to the surface tension σ. Renardy (1987) has noted that even in the absence of an interfacial energy (e.g. $\sigma = 0$) the interfacial displacement must appear in the energy norm for the transient growth calculations to converge. South & Hooper (1999) have verified this in two-dimensional (i.e. $\beta = 0$) calculations of transient growth in two-fluid channel flow for the case $r = 1$. In contrast, we find good convergence even as $\sigma \to 0$, but encounter difficulties in other regimes, such as at very large Re, when the numerical representation of the continuous spectrum becomes very dense in the complex-ω plane.

We now define the growth factor:

$$G(t) = \sup_{\boldsymbol{q}(0)\neq 0}\frac{||\boldsymbol{q}(t)||_E^2}{||\boldsymbol{q}(0)||_E^2} = ||\mathrm{e}^{\mathrm{i}\mathscr{L}t}||_E^2, \quad (4.2)$$

where $\boldsymbol{q}_0$ is an initial disturbance and $\mathscr{L}$ is the linear operator defined above. The maximum or optimal growth is defined as $G_O = \sup_{t\geqslant 0} G(t)$, occurring at time t_O where $G_O = G(t_O)$, while a *peak* value $G_P \equiv \sup_{\alpha,\beta} G_O(\alpha,\beta)$ can also be computed, occurring at α_P, β_P such that $G_P = G_O(\alpha_P, \beta_P)$.

The quantity $G(t)$ is computed by approximating the matrix exponential of (4.2) using the first K least-stable eigenmodes, K chosen to achieve convergence. This technique, based on the singular value decomposition, is adopted from Reddy, Schmid & Henningson (1993) and gives both G and the optimal disturbance associated with G; further numerical details can be found in Yecko & Rossi (2004).

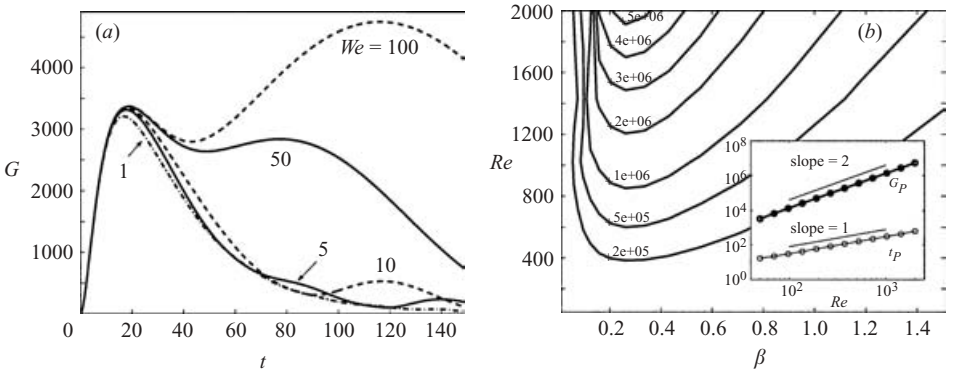

FIGURE 2. (*a*) $G(t)$ for five *We* values at $\alpha = 0$, $\beta = 0.25$, $Re = 50$, $r = 0.0012$, $m = 0.018$; (*b*) G_O values in the (Re, β)-plane at $We = 5.5$, $r = 0.0012$, $m = 0.018$; inset: scaling for G_P and t_P.

5. Results

We adopt the following parameter value ranges: $Re = 50$–2000, $We = 5$–5000, $r = 0.001$–0.07 and $m = 0.01$–0.1, spanning a broad range of liquid–gas combinations and flow regimes, including those of air–water and cryogenic rocket fuel injection. For simplicity, we refer to Re_1, We_1 as Re, We in this section.

5.1. *Parametric dependence of the transient growth*

The streamwise wavenumber of maximum growth always occurs for $\alpha = 0$ (i.e. for disturbances uniform in the streamwise direction); we thus consider only $\alpha = 0$ in this work (but see Yecko 2003). The spanwise wavenumber of maximum growth, β_P, is, however expected to depend on Re, We, r and m. When $\alpha = 0$, each erf profile individually exhibits only a continuous spectrum of modes, similar in behaviour to a Blasius boundary layer. The spectrum of the full problem, however, also contains two discrete modes, corresponding to capillary waves of opposite phase speed propagating on the interface. As explained in § 4, the continuum modes are approximate because of the domain truncation. In addition, we have applied the conditions $v, \mathrm{D}v, \eta \to 0$ rather than the more appropriate boundedness conditions. We have tested this technique on the single-phase Blasius boundary layer, finding excellent agreement with published results, following Butler & Farrell (1992), who also found that vanishing and boundedness conditions gave equivalent results.

To illustrate the nature of the amplification factor defined in equation (4.2), we show in figure 2(*a*) the quantity $G(t)$ computed at five different Weber numbers. We point out that $G(t)$ curves for $We > 100$ are not shown as they cannot be easily distinguished from the curve for $We = 100$ on the plot. Surface tension thus has little influence on the wavenumber or magnitude of peak transient growth. As evident in the multiple peaks seen in figure 2(*a*), however, there may be a powerful indirect effect on the transient growth.

From (4.2), we see that the total energy G is comprised of a liquid kinetic energy, a gas kinetic energy and an interfacial component. Energy is not equipartitioned – the interfacial component is generally small compared to the total energy. In addition, most of the transient energy is found in the normal vorticity component, in the form of streamwise velocity streaks associated with the lift-up effect (Schmid & Henningson 2000), as for single-phase flow. Oscillations due to interfacial modes can, however, become prominent at large values of We, as we have seen in figure 2(*a*) (see also

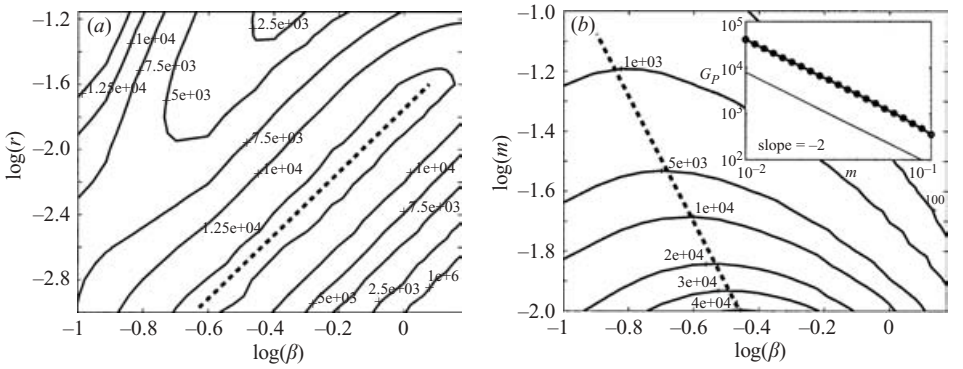

FIGURE 3. (*a*) G_O values in the (r, β)-plane at $Re = 100$, $We = 5.5$, $m = 0.018$; (*b*) G_O values in the (m, β)-plane at $Re = 100$, $We = 5.5$, $r = 0.0012$; inset: scaling of G_P.

Olsson & Henningson 1995). These oscillations can sometimes lead to multiple peaks of comparable magnitude, although typically the local maximum of $G(t)$ that occurs at the earliest time is also the global maximum in time. In this work, we always take the earliest maximum to represent the optimal value G_O.

In figure 2(*b*) we show the maximum growth factors G_O in the (β, Re)-plane. The spanwise wavenumber where peak growth occurs remains relatively constant over a wide range of Re; for example: $\beta_P = 0.25$ at $Re = 50$, while $\beta_P = 0.28$ at $Re = 2000$. Figure 2(*b*) also clearly shows that peak growth factors, G_P, depend strongly on Re. By extracting the maximum values at each Re from the figure, a scaling with Re^2 is found, as for transient growth in single-phase flows. Specifically, $G_P = aRe^2$ (time to achieve peak growth follows $t_P = bRe$); for the case of figure 2(*b*), $a = 1.35$ (and $b = 0.31$) although in general $a = f_a(r, m, We)$ (and $b = f_b(r, m, We)$).

In figure 3(*a*) we map the maximum growth factors G_O over a range of spanwise wavenumber $\beta = 0.1$–1.5 and density ratio $r = 0.001$–0.07. The density ratio r has a strong influence on the spanwise length scale of optimal disturbances. Peak growth falls along a line just below and to the right of the diagonal, as indicated by the dotted line. The slope of this trend implies that the spanwise wavenumber of peak growth follows the relation: $\beta_P \propto r^{1/2}$.

In figure 3(*b*) the quantity G_O is mapped in the wavenumber–viscosity ratio plane, showing a strong dependence of peak growth factors on viscosity ratio, m. The computed scaling derived from the data in figure 3(*b*) is $G_P \propto m^{-2}$. We already know from figure 3(*a*) that G_P does not depend on r but does scale with Re^2. We also found above that G_P is nearly independent of We as long as We is not too small. The scaling seen in figure 3(*b*) thus leads to the relation $G_P = c(Re/m)^2 = cRe_2^2$ since the base flow has the property that $Re_2/Re = 1/m$. Note that the value of $c \approx 4.2 \times 10^{-4}$ is nearly constant. The wavenumber of peak growth also varies with m, as indicated by the dotted line in figure 3(*b*), with dependence $\beta_P \propto m^{-1/2}$.

5.2. *Optimal disturbance structure*

The optimal disturbance fields are easily computed, as mentioned in § 3, from the singular eigenvectors obtained in computing G_O. Figure 4(*a*) shows the optimal disturbance velocity vector $(0, v, w)$, looking downstream, at the time of maximum growth, $t = t_O$. The streamwise velocity component u is shown in figure 4(*b*). At $t = 0$ the optimal disturbance is qualitatively similar, except that $u(t = 0)$ is smaller in magnitude than $u(t = t_O)$ by a factor of order 10^{-2}; the initial optimal disturbance is

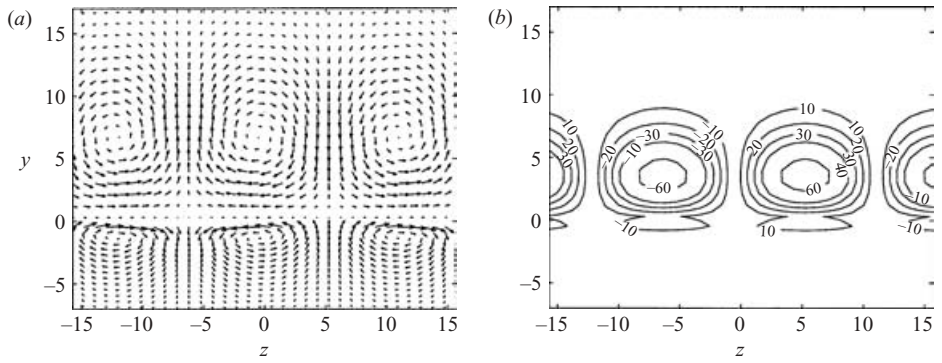

FIGURE 4. Optimal disturbance having $G_O = 13660$, $\beta_O = 0.25$, $t_O = 29.8$ at $Re = 100$, $We = 5.5$, $r = 0.0012$, $m = 0.018$: (*a*) $(0, v, w)$ field; (*b*) $(u, 0, 0)$ field.

thus not shown. In figure 4 the liquid vectors have been magnified by a factor $1/(5r)$ in order to more clearly reveal both liquid and gas quantities in the same plot.

The optimal disturbances clearly exhibit the counter-rotating streamwise vortices familiar from single-phase transient growth. In the two-phase case, the upflows in the liquid extend to the interface and lead to its upward deformation ($f > 0$). These liquid upflows coincide with the gas downflows (figure 4*a*) and are thus found in the same regions where high-speed streaks are produced (figure 4*b*). It therefore appears possible that transient growth may initiate a disturbance field that evolves, in the nonlinear regime, into streamwise oriented ligaments.

5.3. *Comparison with experimental results*

In experiments that exhibit SOL – whether high-speed liquid injected into still gas, or high-speed gas and co-flowing liquid – the SIT assumption is not well founded. For the specific case of high-speed gas and co-flowing liquid, the gas boundary layer develops well upstream of the nozzle. In the region downstream where SOL are observed its shape changes little, while the liquid boundary layer is reversed and then develops. This configuration may be modelled by considering an almost constant gas layer and a liquid layer developing from time zero, the instant zero corresponding to the passage through the nozzle. A base flow that satisfies this has $\delta_1 \propto (\nu_1 t)^{1/2}$ but $\delta_2 \propto (\nu_2(t_0 + t))^{1/2}$, as though the boundary layers had developed from different initial times (DIT). This base flow is a bona fide solution of the Navier–Stokes equation, provided continuity of tangential stresses is imposed, although it is only an approximation of the actual spatially developing flow. We thus relax the SIT assumption. Note that δ_2 will remain nearly constant for times, t, small compared to the characteristic time, t_0, of the already-developed gas boundary layer. It is then possible, within a temporal theory, to examine the effects of the growing liquid boundary layer by computing the flow stability properties over a range of n. This approach is based on the assumption of a nearly constant gas flow, so non-dimensionalization is best performed using U_2^* and δ_2. The five dimensionless parameters are then: Re_2, We_2, r, m, and n. (With the new scaling we denote the resulting G, β values with a † superscript, and, to present dimensional versions, use a * superscript.)

We have computed transient growth properties for several values of n, ranging from $n = 0.2$ to $n = 5$. The results, shown in figure 5(*a*), clearly show that transient growth

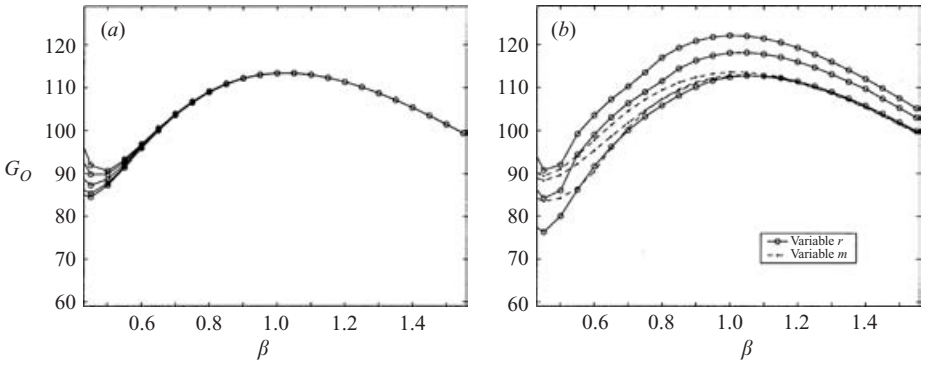

FIGURE 5. (*a*) $G(\beta)$ at $n = 0.2, 0.4, 1.0, 2.5, 5.0$; and (*b*) $G(\beta)$ at $m = 0.02, 0.06, 0.1$ (solid line with circles) and at $r = 0.002, 0.005, 0.01$ (dashed with dots); here $n = 1$.

is independent of n. Since scaling has been performed here with respect to the gas quantities, we find $\beta_P^\dagger \approx 1$. This agrees with the $\beta_P \approx 0.25$ obtained above since under the SIT assumption, $n = (m/r)^{1/2}$ and for air–water, $1/n \approx 1/\sqrt{15} \approx 0.25$.

In figure 5(*b*), we show transient growth factors $G_O^\dagger(\beta^\dagger)$ at several values of r and m, all superimposed. When scaled using δ_2, the previously seen variations of β_P are no longer present. The small variations in β_P and G_P seen in figure 5(*b*) are due to the variations of Re_1 that accompany the variations of m and r.

This agrees with the experimental observation that the ligament length scale does not depend on the liquid layer properties. A spanwise wavenumber of $\beta_P^* = \beta_P^\dagger/\delta_2$ implies a pattern spacing (i.e. distance between ligaments) of $\lambda_P^* = 2\pi/\beta_P^*$. A co-axial jet of (liquid) diameter $d_1 = 7.5\,\text{mm}$, having $\delta_2 \sim 0.2\,\text{mm}$ (Raynal 1997; MV) would thus exhibit approximately seventeen ligaments around the jet circumference, nearly equal to the number seen in experiments, assuming the difference of geometry can be ignored. Since we find $\beta_P^\dagger$ independent of n, r and Re and surface tension influence is small, the predicted ligament number is just inversely proportional to the width of the gas boundary layer.

6. Conclusions

Characteristics of transient growth in a two-phase mixing layer were computed, finding that growth factors scale with Re^2, as for single-phase flow, referring to either the liquid or gas Reynolds number. Optimal disturbances were found to be streamwise uniform with spanwise wavenumber given by $\beta_P^* = 1/\delta_2$. Density ratios $r > 0.07$ and viscosity ratios $m > 0.1$ were not considered in this work, so these results are not expected to carry over to fluids of similar density or viscosity. Optimal disturbances consist of streamwise vortices in both phases, leading to prominent high- and low-speed streamwise streaks in the gas juxtaposed with upward deformations of the interface. Taken together, these features suggest that transient growth is a possible mechanism, worthy of further exploration, for the formation of streamwise oriented ligaments. A model for droplet sizes from primary atomization is a critical component of spray modelling applications and a predictive theory for ligament formation is an essential part of such a model. Until detailed flow fields are obtained, either experimentally or from numerical simulations, the role of transient growth in the formation of streamwise oriented structures remains to be verified.

REFERENCES

Bayvel, L. & Orzechowski, Z. 1993 *Liquid Atomization*. Taylor & Francis.

Boeck, T. & Zaleski, S. 2004 Viscous vs. inviscid instability of two phase mixing layers with continuous velocity profile. *Phys. Fluids* submitted.

Butler, K. M. & Farrell, B. F. 1992 Three-dimensional optimal perturbations in viscous shear flow. *Phys. Fluids* A **4**, 1637–1650.

Hoyt, J. W. & Taylor, J. J. 1977 Waves on water jets. *J. Fluid Mech.* **83**, p. 119–127.

Lasheras, J. C. & Hopfinger, E. J. 2000 Liquid jet instability and atomization in a coaxial gas stream. *Annu. Rev. Fluid Mech.* **32**, 275–308.

Lasheras, J. C., Villermaux, E. & Hopfinger, E. J. 1998 Break-up and atomization of a round water jet by a high-speed annular air jet. *J. Fluid Mech.* **357**, 351–379.

Lefebvre, A. H. 1989 *Atomization and Sprays*. Taylor & Francis.

Lin, S. P. & Reitz, R. D. 1998 Drop and spray formation from a liquid jet. *Annu. Rev. Fluid Mech.* **30**, 85–105.

Lozano, A., Barreras, F., Hauke, G. & Dopazo, C. 2001 Longitudinal instabilities in an air-blasted liquid sheet. *J. Fluid Mech.* **437**, 143–173.

de Luca, L., Costa, M. & Caramiello, C. 2002 Energy growth of initial perturbations in two-dimensional gravitational jets. *Phys. Fluids* **14**, 289–299.

Mansour, A. & Chigier, N. 1990 Disintegration of liquid sheets. *Phys. Fluids* A **2**, 706–719.

Marmottant, P. & Villermaux, E. 2004 On spray formation. *J. Fluid Mech.* **498**, 73–111.

Mayer, W. O. H. 1994 Coaxial atomization of a round liquid jet in a high speed gas stream: A phenomenological study. *Exps. Fluids* **16**, 401–410.

van Noorden, T. L., Boomkamp, P. A. M., Knaap, M. C. & Verheggen, T. M. M. 1998 Transient growth in parallel two-phase flow: Analogies and differences with single-phase flow. *Phys. Fluids* **10**, 2099–3001.

Olsson, P. J. & Henningson, D. S. 1995 Optimal disturbance growth in watertable flow. *Stud. Appl. Maths* **94**, 183–210.

Raynal, L. 1997 Instabilité et entraînement a l'interface d'une couche de mélange liquide-gaz. PhD Thesis, Université Joseph Fourier, Grenoble.

Reddy, S. C. & Henningson, D. S. 1993 Energy growth in viscous channel flows. *J. Fluid Mech.* **252**, 209–238.

Reddy, S. C., Schmid, P. J. & Henningson, D. S. 1993 Pseudospecta of the Orr-Sommerfeld operator. *SIAM J. Appl. Maths* **53**, 15–47.

Renardy, Y. 1987 The thin layer effect and interfacial stability in a two-layer Couette flow with similar liquids. *Phys. Fluids* **30**, 1627–1637.

Sarpkaya, T. & Merrill, C. F. 2001 Spray generation from turbulent plane water wall jets discharging into quiescent air. *AIAA J.* **39**, 1217–1229.

Schlichting, H. & Gersten, K. 2000 *Boundary Layer Theory*, 8th edn. Springer.

Schmid, P. J. & Henningson, D. S. 2000 *Stability and Transition in Shear Flows*. Springer.

South, M. J. & Hooper, A. P. 1999 Linear growth in two-fluid plane Poiseuille flow. *J. Fluid Mech.* **381**, 121–139.

Stapper, B. E., Sowa, W. A. & Samuelson, G. S. 1992 An experimental study of the effects of liquid properties on the breakup of a two-dimensional liquid sheet. *J. Engng Gas Turbines Power* **114**, 39–45.

Wu, P.-K., Miranda, R. F. & Faeth, G. M. 1995 Effects of initial flow conditions on primary breakup on nonturbulent and turbulent round liquid jets. *Atomiz. Sprays* **5**, 175–196.

Yecko, P. 2003 Disturbance growth in primary atomization *Proc. 3rd Intl Conf. on Liquid Atomization and Spray Systems, ICLASS-03, Sorrento, Italy*.

Yecko, P. & Rossi, M. 2004 Instability and transient growth in rotating boundary layers. *Phys. Fluids* **16**, 2322–2235.

Yecko, P., Zaleski, S. & Fullana, J.-M. 2002 Viscous modes in two-phase mixing layers. *Phys. Fluids* **14**, 4115–4123.